Journal of Materials Chemistry A

PAPER

Multidomain simulations of coated ferroelectrics exhibiting spatially selective photocatalytic activity with high internal quantum efficiencies

James J. Glickstein, Paul A. Salvador* and Gregory S. Rohrer

The internal quantum efficiency (IQE) of multidomain ferroelectric BaTiO$_3$ coated with thin (10 nm) anatase TiO$_2$ films has been modeled in two dimensions, using physically reasonable property values of each material. The minority carrier current density averaged across the entire surface, composed of equal portions of positively and negatively polarized domains separated by 180° boundaries, is similar to that reported previously for a single negatively polarized domain (modeled in one dimension). This indicates that photogenerated carriers driven away from the surface in one domain can be collected at the surface of the neighboring domain and participate in surface reactivity. For a wide range of physically reasonable domain widths, from approximately 100 to 400 nm, the limiting IQE is more than 90% of the maximum value, and far exceeds that for Z-scheme domain reactivity, where the carriers driven away from the surface would recombine in the bulk. When the potential and the domain width of alternating positively and negatively polarized domains are optimized, the balancing reduction and oxidation currents occur on the surface with a total limiting IQE as high as 90%, implying there exists significant room for improvement of photocatalysts using spatially varying internal fields at or near the reactive surface.

Introduction

Photocatalytic water splitting has the potential to satisfy a significant portion of the growing global demand for energy.[1] This renewable process requires primary inputs of solar energy, water, and photocatalysts to produce hydrogen fuel. Using existing photocatalysts, however, the solar to chemical energy conversion efficiencies are too low to be competitive with other technologies.[2] One promising approach to developing more efficient photocatalysts is to use materials that contain internal electric fields,[3] which act to separate charge carriers and reduce recombination. Certain materials, such as ferroelectrics, naturally contain internal fields that vary across the surface. The internal fields in ferroelectrics arise from their spontaneous polarization, which varies in orientation for different domains. Oppositely oriented ferroelectric domains have been shown to promote electron and hole currents on different areas of a surface.[4] This spatial selectivity of photochemical reactions allows complete water splitting to proceed on a single surface with the two half-reactions being separated to limit any back-reactions of intermediates.

Ferroelectric domain-specific reactivity has been demonstrated using marker reactions on the surface of illuminated ferroelectric BaTiO$_3$.[5,6] When submersed and illuminated in

Department of Materials Science and Engineering, Carnegie Mellon University, 5000 Forbes Ave., Pittsburgh, PA 15213-3890, USA. E-mail: paul7@andrew.cmu.edu; Tel: +1-412-268-2702

silver nitrate solution, solid Ag reaction products were observed on select domains on the surface. When the surface was cleaned and submersed under illumination in lead acetate solution, solid Pb-containing products were decorated on complementary domains. In a subsequent study,[7] BaTiO$_3$ was coated with a thin TiO$_2$ film to protect from Ba leaching over time.[8–10] The reaction on the surface of the TiO$_2$ coating had a spatial selectivity that was similar to the bare BaTiO$_3$ substrate.[11] Additionally, no significant dependence of the reactivity on crystal orientation was observed for both the bare and coated substrate.[12] Furthermore, heterostructured microcrystalline (Ba,Sr)TiO$_3$ powder photocatalysts coated with nano-crystalline TiO$_2$ shells were shown to have enhanced photochemical hydrogen production rates compared to their individual components.[13]

For both the BaTiO$_3$ (ref. 5 and 6) and TiO$_2$/BaTiO$_3$ (ref. 7, 11 and 12) materials, it was shown that positive ferroelectric domains favored reduction at the surface and negative domains favored oxidation. Because very little photogeneration is expected to occur in the thin TiO$_2$ film, it was also proposed that carriers travel from the substrate through the film to react on the coating surface,[11] which was in agreement with the similar spatially dependent reactivities of the coated and uncoated surfaces. Similar findings were also observed on the surface of TiO$_2$ coatings on BiFeO$_3$, a visible light absorbing ferroelectric.[14] Spatially selective reactivity has also been observed on (111) SrTiO$_3$ surfaces with differently charged terminations.[15,16] Spatial selectivity was found to be associated with the different

This journal is © The Royal Society of Chemistry 2016

J. Mater. Chem. A, 2016, **4**, 16085–16093 | **16085**

surface terminations and was correlated to the measured surface potential. This demonstrates that multiple sources of internal fields can drive the separation of oxidation and reduction reaction products on the surface.

These marker reaction studies of spatially selective reactivity have been largely qualitative in nature, but a quantitative analysis is required to estimate and optimize the performance. We have recently developed and reported on a one-dimensional (1D) computational model designed to improve understanding and to quantify the performance of individual domains in coated ferroelectric semiconductors.[17] The internal quantum efficiency (IQE) of $TiO_2/BaTiO_3$ heterostructures from physical marker reaction literature results was estimated to be below 1%.[17] Simulations showed that the IQE could be increased to over 90% by increasing the reduction reaction kinetics, increasing the carrier lifetime, and optimizing the potential used in the model (all within physically attainable values).[17] However, the >90% IQE was based on separate evaluations of the reduction reactions on individual positively polarized domains and oxidation reactions on individual negatively polarized domains (in both cases the alternate carrier was collected at the back contact, similar to a photoelectrochemical cell electrode). The question related to photocatalytic powder reactors is: how do charge carriers photogenerated in adjacent domains with different polarizations behave? Two limiting possibilities are that the photogenerated charge carriers driven away from the surface either (1) reach the surface of the adjacent domain to react or (2) recombine with one another to be lost, similar to a Z-scheme photocatalyst. The maximum IQE for the first case would be similar to the 1D case, ≈90%, while the maximum IQE of the Z-scheme photocatalyst would be 1/2 of the 1D case, ≈45%.

In this work, we developed a two-dimensional (2D) model to simulate multidomain coated ferroelectric photocatalysts. Variations in surface majority and minority carrier currents were determined across different domains at the illuminated open-circuit potential. These results are particularly relevant in the case of a colloidal catalyst, where the reactions occur in open-circuit conditions at a potential controlled by the solution. The influence of the electric potential on minority carrier currents between oppositely polarized domains is examined. Additionally, the dependence of the surface minority carrier current on domain width is determined. By controlling key parameters, including domain width and the potential, an optimal IQE for balancing oxidation and reduction reactions across the surface as high as 90% is demonstrated, far exceeding a Z-scheme mechanism and nearly equaling the optimal 1D model performance.

Experimental

The 2D model geometry used in this study is depicted in Fig. 1. The lateral position is defined as the position parallel to the film surface, while the depth is defined as the position perpendicular to the surface. The film was modeled as a donor-doped anatase TiO_2 film being 10 nm thick. The donor doped ferroelectric $BaTiO_3$ substrate was modeled as being 1000 nm (1 μm)
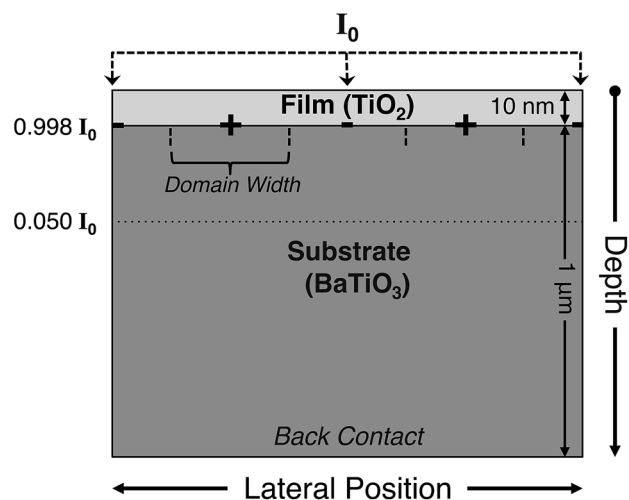

Fig. 1 Schematic of the heterostructure 2D model geometry, with transmitted fractions of the incident irradiance (I_0) indicated.

thick, to provide sufficient space for all light to be absorbed. The spatially varying polarization was applied along the substrate–film interface, switching between positive and negative values of the spontaneous polarization magnitude of $BaTiO_3$ ($P_{BTO} = \pm 26$ μC cm^{-2}).[18] For simplicity, the width of positive and negative domains was always equal and the spontaneous polarization was aligned to be normal to the surface. These 180° domain boundaries are marked as dashed lines at the interface in Fig. 1.

The computational model used in this work was developed in the commercial finite element software package COMSOL Multiphysics®.[19] The equations and variables incorporated into the model have been described explicitly elsewhere.[17,20] The electrostatic potential and carrier (electron and hole) concentrations are solved throughout the geometry using Poisson's equation, carrier current continuity equations, and carrier drift and diffusion equations. The material parameter values for TiO_2 (anatase)/$BaTiO_3$ heterostructures have been extracted from the literature,[21–38] and are largely identical to those presented in the 1D study,[17] except where noted below. The carrier lifetime was set to 100 ns (a physically achievable value[39]), which was required, along with a high effective Richardson constant for electrons (A_n^*), to enable efficiencies exceeding 90% in the 1D model.[17]

Light (of sufficiently energetic photons) was modeled as being uniformly incident at the film surface with an irradiance of I_0 (set to the estimated value from physical experiments from the literature of 1×10^4 W m^{-2}) and as being absorbed according to the Beer–Lambert law, resulting in a transmitted irradiance of $0.998I_0$ (0.2% absorbed) at the film–substrate interface and $0.050I_0$ (95% absorbed) at a depth (below the film surface) of 310 nm. Assuming that all of the absorbed photons photogenerate charge carriers, the irradiance sets an upper limit of 262 mA cm^{-2} on the photogenerated current density. This limit applies primarily to minority carriers (holes), which are nearly entirely photogenerated. Majority carriers (electrons) are present in high concentrations and can be driven to the surface by electric fields, generating currents that far exceed the

16086 | *J. Mater. Chem. A*, 2016, **4**, 16085–16093

This journal is © The Royal Society of Chemistry 2016

photogenerated limit. Shockley–Read–Hall recombination is applied throughout the model, with the recombination rate being dependent on the carrier lifetimes and local carrier concentrations.

The reactive film surface was modeled as a Schottky contact, which simulates equilibration of the photocatalyst with a solution (at a fixed potential). Thermionic emission governed charge transfer across the surface, and the effective Richardson constant of the Schottky contact was used as a kinetic parameter in this model to regulate the rate at which charge carriers near the surface react. In this work, the effective Richardson constants were set to 1×10 A m^{-2} K^{-2} for holes and 1×10^7 A m^{-2} K^{-2} for electrons, consistent with the physically reasonable optimized results presented in the 1D study.[17] In this way, the kinetics of the oxidation reaction are set to those values predicted from published marker reaction data and the reduction reaction kinetics are set to the maximum theoretical value (this can be achieved physically by the addition of a co-catalyst). At the solid interface between the film and substrate, thermionic emission governed charge transfer and a local static charge density was implemented to simulate the ferroelectric spontaneous polarization. The back edge of the substrate was modeled as an ohmic contact. The potential was controlled by applying a voltage to the back ohmic contact relative to the fixed potential at the film surface. The open-circuit voltage under illumination (V_{OC}^*) was estimated to be -0.3 V vs. SCE, just anodic of the flat-band potential. Applied potentials alter the surface band bending and preferentially favor increased oxidation or reduction currents relative to the illuminated open-circuit voltage.

The most important metrics for evaluating the simulated multidomain photocatalytic performance are the spatially varying electron and hole currents, as well as their surface averages. The variation in surface currents with lateral position reveals the location and rate at which oxidation and reduction reactions are expected to occur and the extent of domain-specific reactivity can be readily observed. The surface average currents, computed by integrating the current for a single carrier across the film surface, can be used to determine the overall efficiency of a given half reaction over the total illuminated area. The lower of the reductive and oxidative surface average currents represents the limiting half reaction, and can be used to determine the overall IQE of the water-splitting reaction.

Results

The previously reported marker reaction data from thin TiO$_2$ films on BaTiO$_3$ (ref. 11) is reproduced in Fig. 2a and b for oxidation and reduction reactions, respectively. These figures display domain-specific reactivity on the surface of a 15 nm film. The illuminated heterostructure was submersed in an aqueous lead acetate solution in Fig. 2a, with the areas of bright contrast representing solid PbO$_2$ oxidation reaction products. The same illuminated surface was submersed in aqueous silver nitrate solution in Fig. 2b, with bright contrast now representing solid Ag reduction reaction products. The reaction products

for each half-reaction appear to be segregated to specific, complementary, ferroelectric domains. While quantitative reaction rates are difficult to determine from these experiments, because the surface becomes coated during testing, the submersed sample had to be illuminated for 18 times as long to produce a comparable height of oxidation products (Fig. 2a) as reduction products (Fig. 2b), indicating that the oxidation reaction is slower. The average domain width from these physical materials was estimated to be ≈ 250 nm. The domain boundary angles in the physical samples vary, with a high concentration of 90° boundaries visible in Fig. 2a and b. The simulations herein were carried out using 180° domains, which model the maximum difference in the normal component of the polarization for neighboring domains.

The simulated surface oxidation (hole) and reduction (electron) currents, evaluated at V_{OC}^* for 250 nm domains and a 10 nm film, are shown in Fig. 2c and d, respectively. The full simulated surface geometry was 1000 nm but, for simplicity, only 500 nm of the surface are shown: half of a positively polarized domain, a full negatively polarized domain, and another half of a positive domain (the domain boundaries are given as vertical dashed lines). The surface average currents ($J_{p,n}^{avg}$) are obtained by integrating across the displayed 500 nm of the surface. In Fig. 2c, the maximum photogenerated current (J_{ph}^{max}) and twice the maximum photogenerated current ($2J_{ph}^{max}$) are also shown as horizontal dotted lines. The maximum photogenerated current, fixed by the irradiance to be 262 mA cm^{-2}, is the maximum possible value of the surface average hole current density. It can be exceeded by the local hole current density, however, if lateral driving forces are present that allow holes to accumulate in certain regions on the surface. The $2J_{ph}^{max}$ current represents the value if all photogenerated holes uniformly reacted on the surface of the negative domain (1/2 of the total surface).

Examining Fig. 2c, the hole current is nearly zero (<1 mA cm^{-2}) at the surface of positive domains, increases near the domain boundary, and peaks above 420 mA cm^{-2} at the center of the negative domain. The domain-specific simulated hole current in Fig. 2c is qualitatively comparable to the observed physical reactivity of Pb^{2+} oxidation in Fig. 2a. The current density throughout the majority of the negative domain exceeds J_{ph}^{max}, but never exceeds $2J_{ph}^{max}$. The ratio of J_p^{avg} to J_{ph}^{max} can be used to calculate an IQE for the minority carrier reaction, being 69% for this simulation, confirming a performance that exceeds a pure Z-scheme (which could never be higher than 50%).

This result is very promising, assuming that the positive domains can also promote the complementary reduction reaction. Fig. 2d displays the spatial variation of the electron current density (J_n) and its surface average (J_n^{avg}). Reductive electron currents are negative by convention, so the absolute value is plotted here for direct comparison with the hole currents. The domain-specific simulated electron surface current shown in Fig. 2d is qualitatively comparable to the observed physical reactivity of Ag$^+$ reduction in Fig. 2b, and is complementary to the hole current shown in Fig. 2c. The magnitude of the current density is very low across the majority of the negative domain (<10 mA cm^{-2}), increases sharply near the boundary to a peak
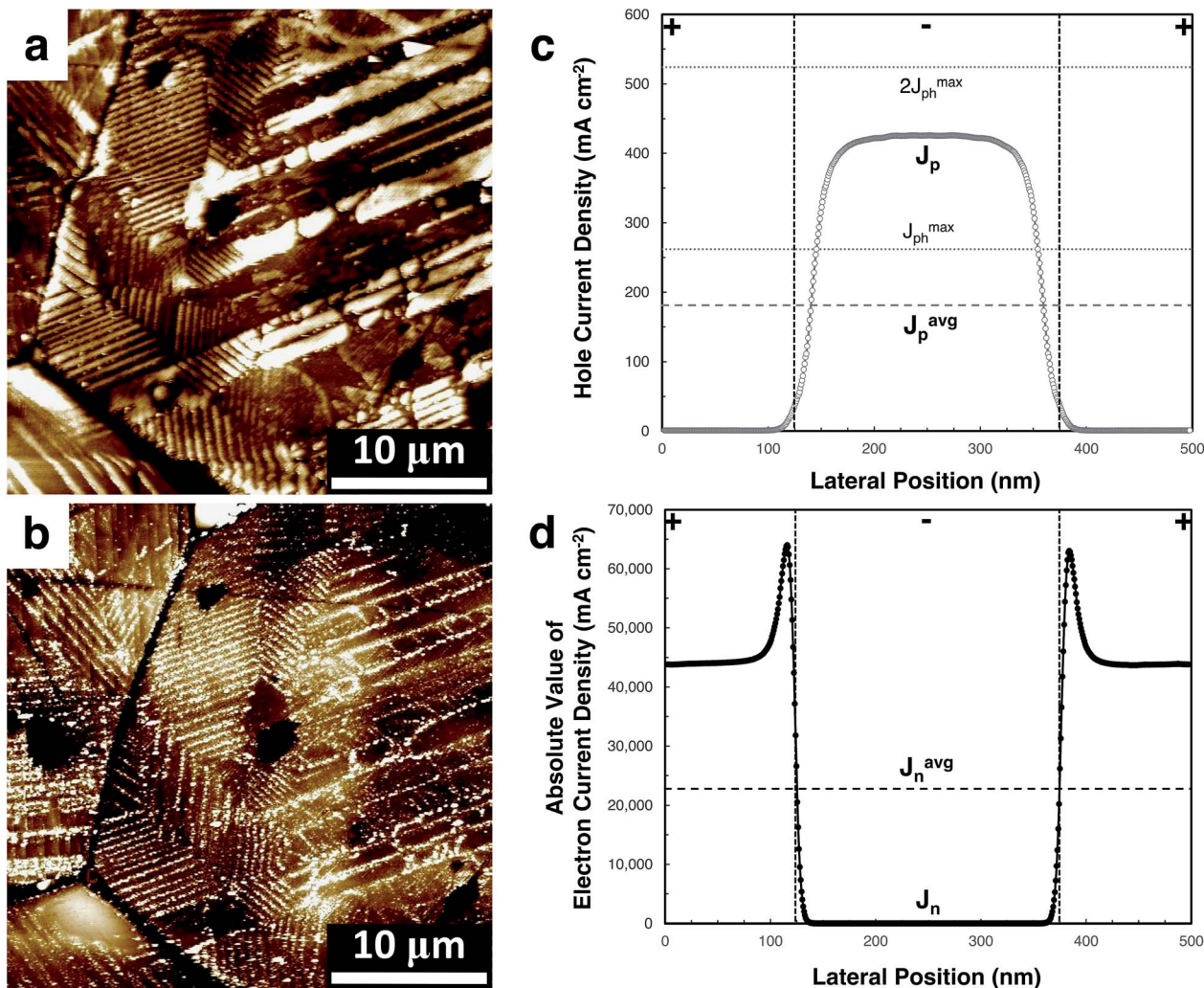
Fig. 2 Comparison of experimental marker reaction data (a and b)[†] and simulated faradaic current variation across the surface (c and d) for oxidation (a and c) and reduction (b and d) reactions. Experimental results are for an illuminated 15 nm TiO_2 film on $BaTiO_3$ exposed to aqueous lead acetate solution (a) and aqueous silver nitrate solution (b), while simulated photoelectrochemical results are for an illuminated 10 nm TiO_2 film on $BaTiO_3$ fixed at V_{OC}^* with alternating 250 nm wide negative and positive domains. [†] Parts (a) & (b) reproduced from ref. 11.

value above 63 000 mA cm^{-2} on the edge of the positive domain, and settles to a value close to 44 000 mA cm^{-2} near the center of the positive domain. These values for J_n on positive domains greatly exceed J_{ph}^{max}, and are the result of the relatively cathodic bias and substantial donor density in the catalyst heterostructure. The significantly higher order of magnitude for electron current densities at the illuminated open-circuit potential (V_{OC}^*) compared to hole current densities parallels the much faster rate of production of marker reaction products for reduction compared to oxidation.[11] Additionally, the accumulation of the electron current near the boundaries of positive domains is comparable to physical marker reaction observations for 180° domain boundaries that show deposits concentrated near the boundaries.[12] Finally, in comparing the quantitative results from Fig. 2c and d, it is clear that the net reaction on negative domains is oxidation and the net reaction on positive domains is reduction, with oxidation on the negative domains limiting the overall reaction across the entire surface.

The results from Fig. 2c strongly suggest the existence of lateral driving forces that promote the transfer of minority carriers from positive to negative domains. Fig. 3a plots the hole concentrations and electric fields in a 250 nm wide and 100 nm deep region of the model, containing a domain boundary in the middle separating halves of negative and positive domains. The grayscale gradient denotes the log of the local hole concentration (which drives diffusion currents) and the arrows indicate the local direction of the electric field acting on a positive charge (which drives drift currents). The arrow length is logarithmically proportional to the electric field magnitude. In the substrate, there is a semi-circular electric field that drives holes photogenerated in the positive domain of the substrate (99.8% of absorption occurs in the substrate) across the domain boundary and towards the solid interface in the negative domain. This results in a greater than four orders of magnitude difference in the hole concentration near the solid interface in the positive domain compared to in the negative domain.
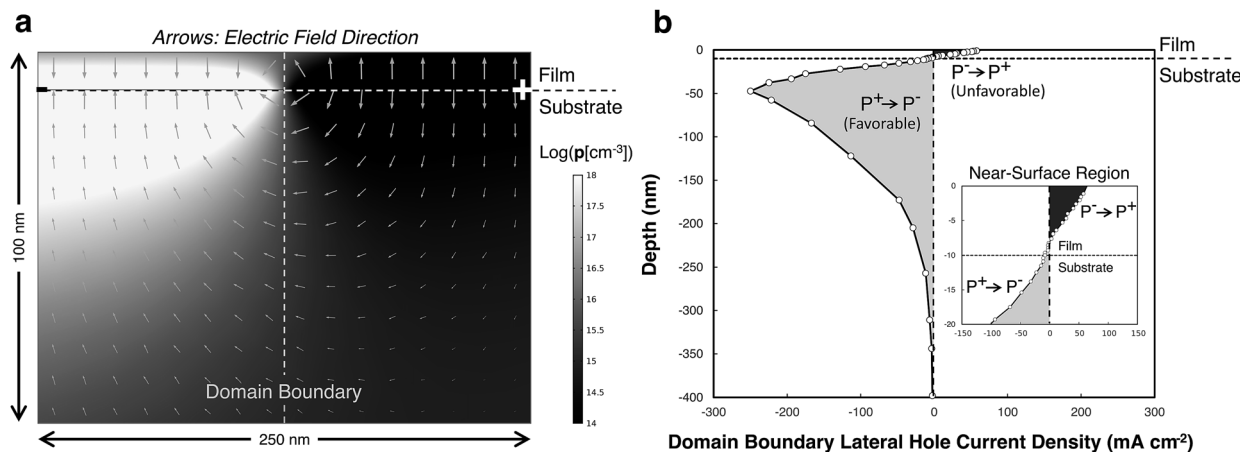
Fig. 3 (a) Simulated steady-state hole concentration distribution at V_{OC}^{*} in the vicinity of a domain boundary between 250 nm wide negative and positive (half) domains. Arrows indicate the spatial variation of the electric field direction (acting on a positive charge), with the length of the tail being logarithmically proportional to the electric field magnitude at each coordinate. (b) Variation in the lateral hole current density (J_{p}^{x}) at the domain boundary with depth. Negative J_{p}^{x} values correspond to hole transfer from positive to negative domains and positive J_{p}^{x} values represent hole transfer from negative to positive domains.

Within the film on the negatively polarized substrate, the electric field actually drives holes away from the surface and back towards the solid interface, but the high hole concentration near the interface leads to diffusion currents that result in a net hole current at the surface.

The lateral hole currents across the domain boundary are quantified in Fig. 3b, with hole transfer from positive to negative domains defined as negative lateral hole current and transfer from negative to positive domains defined as positive lateral hole current. Transfer from positive to negative domains is considered favorable, because it contributes to decreasing recombination and separating oxidation and reduction reactions to oppositely polarized domains. The lateral transfer throughout the substrate is entirely favorable and peaks near a depth of 50 nm (with a magnitude of 250 mA cm^{-2}) before attenuating to negligible lateral transfer at a depth of 400 nm. There is a net lateral transfer of holes in the opposite direction in most of the film, representing unfavorable (leakage) current. Though the electric field direction from Fig. 3a favors hole transfer from positive to negative domains within the film, the diffusion current dominates and there is a net leakage across the film boundary. However, this leakage transfer is significantly lower than the favorable boundary transfer of holes from positive to negative domains throughout the substrate depth.

It is evident from Fig. 3 that the polarization gives rise to a strong driving force for charge transfer across domain

boundaries, which enables an efficiency that is not limited by a Z-scheme. Table 1 summarizes the variation in the surface average hole current density and corresponding limiting IQE for different multiples of the BaTiO$_3$ polarization magnitude. There is a significant increase in the IQE from the zero polarization case for even one quarter of P_{BTO}. The IQE increases with increasing polarization but with diminishing returns as the polarization increases.

With the minority carrier transfer between domains being of extreme importance in producing high efficiencies, it is important to evaluate how the domain width affects this transfer. Fig. 4a displays the surface average hole current density for a variety of different domain widths, spanning two orders of magnitude from 10 to 1000 nm. The Z-scheme line marks the value (90 mA cm^{-2}) that represents half of the 1D simulated performance for a negative domain (180 mA cm^{-2}). For very low domain widths, J_{p}^{avg} is below the Z-scheme line. The surface average hole current sharply increases with increasing domain width before reaching a peak value near 180 mA cm^{-2} (the 1D J_p for a negative domain). There is a wide range of physically reasonable domain widths, including 100–400 nm, that are above 90% of the maximum value, including the 250 nm domains used to produce Fig. 2 and 3. As the domain width is increased further, the surface average hole current gradually decreases. It is expected that J_{p}^{avg} will eventually approach the Z-scheme line for sufficiently wide domains, representing the width at which any lateral transfer at domain boundaries no longer has a significant impact on the surface average currents. Nevertheless, even at 1 μm domain widths, the IQE is still above the Z-scheme value.

An analysis of the electric potential variation across the solid interface for small domain widths provides an explanation for the decreasing surface average hole current below a width of 100 nm. The oppositely oriented polarization-induced electric fields, when placed in close proximity, partially cancel each other out for very narrow domains, as can be seen in Fig. 4b for

Table 1 Variation in surface average hole current and corresponding IQE with polarization magnitude

	$P_{BTO} = \pm 26$ μC cm^{-2}				
	0	$0.25P_{BTO}$	$0.5P_{BTO}$	P_{BTO}	$2P_{BTO}$
J_{p}^{avg} (mA cm^{-2})	54	100	130	180	220
IQE (%)	21	38	50	69	84

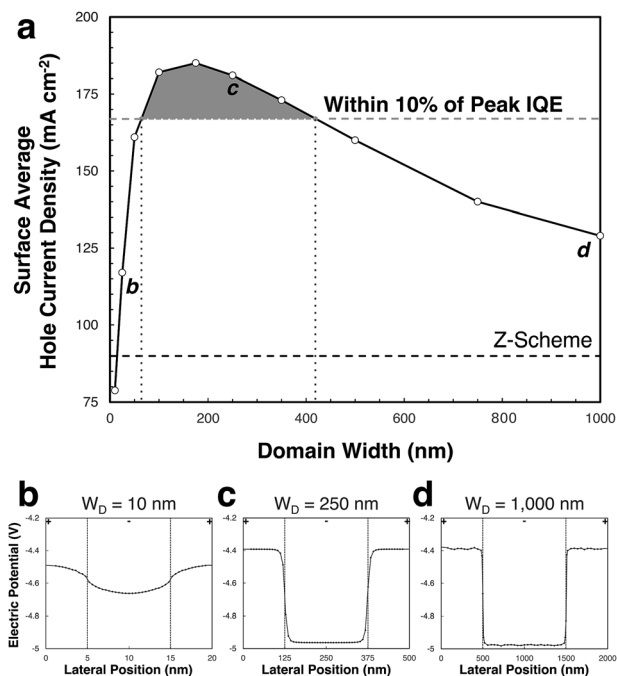Fig. 5 Simulated electron (J_n) and hole (J_p) currents across the surface for 250 nm domains at V_{opt}.

Fig. 4 (a) Simulated dependence of the surface average hole current density on domain width at V_{OC}^*. (b–d) Electric potential variation with lateral position for 10 nm (b), 250 nm (c), and 1000 nm (d) domain widths.

10 nm domains. The difference in electric potential measured at the solid interface (where the polarization is applied) between the center of negative and positive domains is only 0.17 V for a 10 nm domain, compared to 0.60 V for a 250 nm domain, shown in Fig. 4c. As is evident from Fig. 4d, the electric potential difference between negative and positive domains is the same (0.60 V) for 1000 nm wide domains as it is for 250 nm domains, with the only difference in electric potential being that the boundary transition region constitutes a smaller percentage of the total domain width for 1000 nm domains. This illustrates that, as the domain width is increased, the difference in electric potential quickly reaches a maximal value (0.6 V in this simulation). The effects of decreasing electric potential gradients for narrower domains and lower values of lateral currents across domain boundaries for wider domains are balanced within the shaded region in Fig. 4a, where the currents are above 90% of the 1D value. It should be noted that the minority carrier lifetime, which was fixed in this work, will affect the recombination rate at the larger domain sizes, resulting in a decreased IQE with a decreasing lifetime.

The simulations thus far show that the multidomain IQE greatly exceeds a pure Z-scheme performance and that 250 nm domains are the near-optimal domain width (for the values investigated). In the previously reported 1D simulations,[17] the IQE was a strong function of the applied potential. The data presented thus far in the 2D model was simulated at −0.3 V vs. SCE, the estimated illuminated open-circuit potential. However, at this potential, the electron current magnitude far exceeds the hole current magnitude (as shown in Fig. 2), and the hole current is the limiting half-reaction. If the anodic bias is increased until the surface average currents become nearly
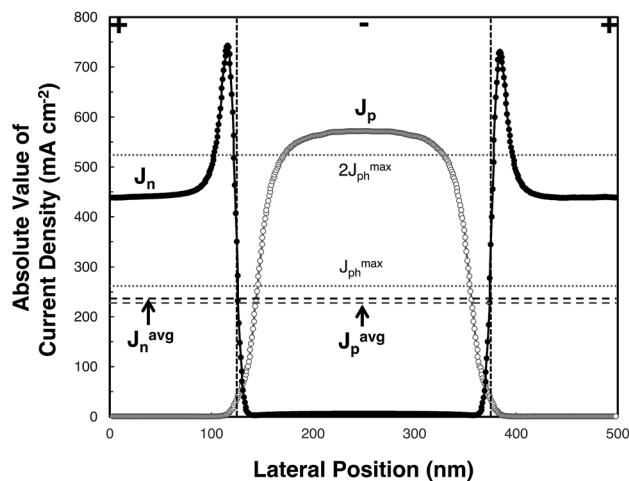
equal, a more optimal performance can be obtained. In the 1D model, application of a small anodic potential resulted in an IQE of over 90%.[17]

The absolute value of the electron and hole current densities for 250 nm domains are displayed in Fig. 5 at an optimal potential (V_{opt}) of −0.135 V vs. SCE (+0.165 V vs. V_{OC}^*). The electron current is significantly lower in magnitude but takes the same general shape as in Fig. 2d, with the highest current being near the domain boundaries. The surface average electron current magnitude is reduced to 240 mA cm^{-2}. The surface average hole current magnitude is increased to just below that of electrons, at 230 mA cm^{-2}. At this more positive voltage, the hole current density actually exceeds $2J_{ph}^{max}$ at the center of the negative domain (this is possible because the current density does not take the precise shape of a step function). At this voltage the electron and hole currents are nearly equal and the limiting (hole) current has been increased, resulting in an enhanced IQE of 88%. The voltage adjusted IQE is 76%; which still exceeds the open circuit values. In a particulate photocatalyst, the optimal potential can be achieved by changing the solution pH to achieve and operate at the full efficiency.

In Table 2, a summary of the surface average electron and hole currents is compared with corresponding 1D results at both V_{OC}^* and V_{opt}. The 1D currents were obtained by using

Table 2 Comparison of hole currents for 1D (single domain) and 2D (multidomain, 250 nm domain width) simulations at illuminated open-circuit and optimal voltages

		Voltage vs. SCE (V)	
		−0.3 (V_{OC}^*)	−0.135 (V_{opt})
J_n (mA cm^{-2})	1D J_n (P$^+$)	−39 000	−250
	2D J_n^{avg}	−23 000	−240
J_p (mA cm^{-2})	1D J_p (P$^-$)	180	240
	2D J_p^{avg}	180	230
2D IQE (%)		69	88

a modified version of the previously described model,[17] and were determined separately for individual negative and positive domains. At the estimated illuminated open-circuit potential, the surface average electron current in 2D is slightly more than half of the 1D value for a positive domain, whereas the surface average for holes in 2D is equal to the 1D value for a negative domain. This results in an overall IQE, limited by the oxidation reaction, of 69%. At the optimal voltage, both the electron and hole surface average currents (in 2D) are marginally below their 1D single domain values, and the overall IQE is increased to 88%. When the slightly higher performing peak domain width (175 nm) is extracted from Fig. 4a and evaluated at -0.135 V $vs.$ SCE, a 2D limiting IQE of 90% is obtained. Therefore, by optimizing the domain width and potential, oxidation and reduction reactions can be spatially separated on adjacent oppositely polarized domains with an overall IQE as high as 90%, far exceeding a pure Z-scheme and nearly matching the predicted combined optimal performance of isolated positive and negative domains. A significant percentage of the remaining losses in the system can be recovered by further increasing the carrier lifetime, to values that may be physically achievable.[39] When the lifetime is set to 0.1 s with the potential and domain width optimized, the IQE is increased to 97%.

Discussion

Coated ferroelectrics that exhibit spatially selective reactivity have the potential to be highly efficient water-splitting photocatalysts by separating the two half-reactions on a single surface. Marker reactions, which are primarily qualitative, have been used previously to demonstrate domain-specific reactivity on the surface of thin TiO_2 coatings on ferroelectric $BaTiO_3$.[11] However, the performance of the samples used to produce the data in Fig. 2a and b has been estimated to have a limiting IQE below 1%.[17] The spatial separation of oxidation and reduction reactions depicted in Fig. 2a and b is evident from the simulated data in Fig. 2c and d. The observation that J_p significantly exceeds J_{ph}^{max} throughout much of the negative domain strongly suggests that minority carriers photogenerated in positively polarized regions are being transferred to negatively polarized regions before ultimately being transferred to the surface. A 1D model of a negative domain (which favors the oxidation reaction) produced a hole current magnitude of 180 mA cm^{-2}, which is approximately equal to the surface averaged value J_p^{avg} in the 2D model, indicating that roughly the same percentage of photogenerated holes are collected whether the surface is one large negative domain or is divided equally into two 250 nm wide oppositely polarized domains. In this way, the local hole current in the multidomain simulations at the surface of a negative domain is actually much higher than that expected for an isolated negative domain. The limiting IQE is 69% at the illuminated open-circuit potential, a value similar to the 1D case and roughly twice that expected from a Z-scheme. Achieving a high carrier lifetime to enable this greatly enhanced efficiency has recently been shown to be feasible in ferroelectrics.[39] Increases in carrier lifetimes of up to four orders of magnitude were observed in $BaTiO_3$, and were attributed to the

reduction in recombination enabled by polarization-induced internal fields.[39] Coupled with the incorporation of a co-catalyst, such as Pt, to improve the reduction kinetics (on the positive domains), these results provide a pathway for designing highly efficient coated ferroelectric photocatalysts.

Fig. 3 enhances the understanding of the mechanism by which minority carriers photogenerated in positive substrate domains are ultimately collected on the surface above negative domains. Electric fields drive high concentrations of holes across the domain boundary towards the solid interface in negative substrate domains, with diffusion ultimately resulting in hole transfer through the film to generate current. Because the polarization induces these driving electric fields, the magnitude of the polarization (or the component of the polarization oriented along the surface normal) has a large influence on the IQE, as seen in Table 1. It is important to note that the polarization dependence is more significant than that seen for single domains,[17] which is attributable to the significance of lateral polarization-induced electric fields on the results of multidomain simulations. It is evident that the polarization magnitude should be maximized to increase the driving force that results in a higher limiting IQE. This is relevant when considering other materials that have a different spontaneous polarization or even a different source of surface charge, such as the charged terminations in coated $SrTiO_3$.[15,16]

This finding is also important when considering a more physically realistic coated $BaTiO_3$ surface that does not contain purely 180° domain boundaries with the polarization oriented normal to the surface. Much of the spatially selective reactivity seen in Fig. 2a and b is across 90° domain walls. Furthermore, the marker reaction product step heights used to estimate an IQE below 1% were measured across 90° domains.[17] For these domain boundaries, the component of the polarization that is normal to the surface can be compared to the model, though the component that is parallel to the surface may also contribute to the lateral charge transfer (those effects are not modeled here). Considering only the component of the polarization that is normal to the surface, these results suggest that spatial selectivity should be more pronounced across 180° domains than 90° domains.

The increase in efficiency from below 1%, estimated for the physical samples, to 69% for simulated 180° domains at open-circuit can be attributed to multiple factors. The first major factor is a low estimated effective Richardson constant for electrons in the physical samples, which results in electrons severely limiting the overall current at the illuminated open-circuit potential (and all more anodic potentials) when the carrier lifetime is 100 ns.[17] If a reduced effective Richardson constant for electrons had been used in this study, the minority carrier currents would be largely unchanged, but the majority carrier currents at more anodic voltages would be significantly reduced and there would be no potentials at which such high efficiencies could be achieved. However, minority carrier currents were also estimated to be low at the illuminated open-circuit potential for the reported data on physical samples.[17] The major factor that contributes to the decreased hole currents in the reported physical results may be the predominance of 90°

This journal is © The Royal Society of Chemistry 2016

J. Mater. Chem. A, 2016, 4, 16085–16093 | **16091**

domains across the surface. The electric fields demonstrated in this work that drive minority carriers across 180° domain walls will be oriented differently for 90° domains, and the distance that minority carriers must travel before reaching the surface will likely be much longer. Therefore, the 250 nm domains that are shown here to be nearly ideal, may be wider than optimal for 90° domains. Furthermore, the normal component of the polarization (which drives carriers to the surface to be collected) is reduced for 90° domains, and this in turn may effectively shorten the carrier lifetime, which has been shown to be enhanced by the ferroelectric polarization.[39] Therefore, to produce physical photocatalysts that can achieve the IQEs demonstrated in this work, the kinetics of the majority carrier reaction must be improved and the domain structure must be designed to minimize the distance that minority carriers must travel before reaching the surface while simultaneously maximizing the polarization-enhanced carrier lifetime.

The concentration of majority carrier current near the domain boundaries revealed in Fig. 2d and 5 sheds light on the predicted distribution of marker reaction products on these surfaces. In the simulations, electrons are swept from negative to positive domains (across 180° domain boundaries) due to the strong electric fields, resulting in the region near the boundaries being the most reactive. Highly reactive 180° domain walls (that are more reactive than the bulk of the domains) have been observed in majority carrier marker reaction experiments conducted on $BaTiO_3$ with and without a TiO_2 coating.[5,12] Enhanced majority carrier reactivity at 180° domain walls has also been observed in another ferroelectric material, $LiNbO_3$, with Ag marker reaction deposits shown to be concentrated at the boundary.[40,41] The enhanced local activity was attributed to the steep gradient in the electric field near the boundary, which is evident for coated $BaTiO_3$ as well from Fig. 4b–d. The minority carrier current density displayed in Fig. 2c and 5, which is also influenced significantly by sweeping electric fields, peaks at the center of negative domains rather than near the boundaries. This occurs because, while majority carriers are present in high concentrations near the surface, minority carriers are photogenerated deeper into the modeled geometry (with minimal photogeneration in the film) and are driven to the surface by the electric field lines shown in Fig. 3a, which are directed towards the center of negative domains.

With lateral minority carrier currents enabling higher efficiencies, it would be logical to hypothesize that narrower domains may lead to increased performance by decreasing the distance that holes must travel before being collected. These long distances do result in losses for wide domains. However, there are two counteracting phenomena that give rise to the peak observed in Fig. 4a. The first is that for very small domain widths, the polarizations are in such close proximity that their effects cancel each other. In the limit of infinitesimal domain widths, the surface currents approach the values for zero polarization, which results in a significantly reduced efficiency. The second balancing phenomena is that, the holes photogenerated in positive domains must travel longer distances without recombining, before being collected at the surface of negative domains, as the domain width increases. When the

domains are wide enough, relative to the carrier lifetime or diffusion lengths, fewer holes photogenerated in the central region of the positive domains should contribute to the surface averaged current, which results in the decreased surface average hole current for 1000 nm domains observed in Fig. 4a. The minority carrier diffusion length, at a 100 ns lifetime, is roughly 250 nm. Minority carriers photogenerated in positive domains must not only be transported across the domain to the boundary, but must then travel through the depth of the heterostructure to the film surface before being collected. This extended minority carrier transport distance is balanced by the drift forces shown in Fig. 3, which are enhanced for wider domain widths. Ultimately, a large range of physically reasonable domain widths from approximately 100–400 nm are desired to balance these two effects. Therefore, the results show that the minority carrier current is maximized approximately where the domain width is equal to the diffusion length.

To increase the IQE beyond 69% for 250 nm domains, the voltage must be optimized to obtain nearly equal electron and hole currents, as shown in Fig. 5. The limiting IQE is improved to 88% at −0.135 V *vs.* SCE. The IQE can be optimized further to 90% by using a slightly reduced domain width and up to 97% by increasing the carrier lifetime to 0.1 s. These relatively small adjustments to the potential (0.165 V) can be achieved without an external bias (which lowers the overall efficiency and would not be practical for a colloidal catalyst) by altering the pH of the solution to reach the desired electrochemical potential. These multidomain simulations provide a framework for obtaining 90% internal quantum efficiencies in coated ferroelectric photocatalysts. The conclusions supported here can be applied to achieve enhanced internal quantum efficiencies in material systems with higher achievable solar-to-hydrogen conversion efficiencies.

Conclusions

A 2D COMSOL® model of thin TiO_2 films on ferroelectric $BaTiO_3$ was shown to produce oxidation currents localized on negative domains and reduction currents localized on positive domains, with an overall efficiency that far exceeds a pure Z-scheme mechanism. The IQE varies by less than 10% over a wide range of domain widths from 100–400 nm. When the domain width and potential are optimized, oxidation and reduction currents are spatially separated to adjacent oppositely polarized domains with an overall IQE as high as 90%.

Acknowledgements

Notes and references

1 B. A. Pinaud, J. D. Benck, L. C. Seitz, A. J. Forman, Z. Chen, T. G. Deutsch, B. D. James, K. N. Baum, G. N. Baum, S. Ardo, H. Wang, E. Miller and T. F. Jaramillo, *Energy Environ. Sci.*, 2013, **6**, 1983.

2 U.S. Department of Energy: Office of Energy Efficiency & Renewable Energy: Multi-Year Research, Development, and Demonstration Plan: 2015 Production Section, http://energy.gov/sites/prod/files/2015/06/f23/fcto_myrdd_production.pdf, accessed February 2016.

3 L. Li, P. A. Salvador and G. S. Rohrer, *Nanoscale*, 2014, **6**, 42.

4 D. Tiwari and S. Dunn, *J. Mater. Sci.*, 2009, **44**, 5063.

5 J. L. Giocondi and G. S. Rohrer, *Chem. Mater.*, 2001, **13**, 241.

6 J. L. Giocondi and G. S. Rohrer, *J. Phys. Chem.*, 2001, **105**, 8275.

7 N. V. Burbure, P. A. Salvador and G. S. Rohrer, *J. Am. Ceram. Soc.*, 2006, **89**, 2943.

8 H. W. Nesbitt, G. M. Bancroft, W. S. Fyfe, S. N. Karkhanis and A. Nishijima, *Nature*, 1981, **289**, 358.

9 A. Neubrand, R. Lindner and P. Hoffmann, *J. Am. Ceram. Soc.*, 2000, **83**, 860.

10 J. H. Adair, J. Crampo, M. M. Mandanas and E. Suvaci, *J. Am. Ceram. Soc.*, 2006, **89**, 1853.

11 N. V. Burbure, P. A. Salvador and G. S. Rohrer, *Chem. Mater.*, 2010, **22**, 5823.

12 N. V. Burbure, P. A. Salvador and G. S. Rohrer, *Chem. Mater.*, 2010, **22**, 5831.

13 L. Li, G. S. Rohrer and P. A. Salvador, *J. Am. Ceram. Soc.*, 2012, **95**, 1414.

14 Y. Zhang, A. M. Schultz, P. A. Salvador and G. S. Rohrer, *J. Mater. Chem.*, 2011, **21**, 4168.

15 J. L. Giocondi and G. S. Rohrer, *J. Am. Ceram. Soc.*, 2003, **86**, 1182.

16 Y. Zhu, P. A. Salvador and G. S. Rohrer, *Chem. Mater.*, 2016, **28**, 5155.

17 J. J. Glickstein, P. A. Salvador and G. S. Rohrer, *J. Phys. Chem. C*, 2016, **120**, 12673.

18 M. E. Lines and A. M. Glass, *Principles and Applications of Ferroelectrics and Related Materials*, Clarendon, Oxford, 1970.

19 *COMSOL Multiphysics® v. 5.1*, COMSOL AB, Stockholm, Sweden, http://www.comsol.com.

20 A. T. Garcia-Esparza and K. Takanabe, *J. Mater. Chem. A*, 2016, **4**, 2894.

21 A. Euken and U. A. Buchner, *J. Phys. Chem. B*, 1934, **27**, 321.

22 S. Roberts, *Phys. Rev.*, 1949, **76**, 1215.

23 R. G. Breckenridge and W. R. Hosler, *Phys. Rev.*, 1953, **91**, 793.

24 C. N. Berglund and W. S. Baer, *Phys. Rev.*, 1967, **157**, 358.

25 H. Tang, K. Prasad, R. Sanjinès, P. E. Schmid and F. Lévy, *J. Appl. Phys.*, 1994, **75**, 2042.

26 N. A. Deskins and M. Dupuis, *J. Phys. Chem. C*, 2009, **113**, 346.

27 P. Günter and H. Jean-Pierre, *Photorefractive Materials and Their Applications I: Fundamental Phenomena, Topics in Applied Physics*, Springer-Verlag, Berlin, 1988.

28 Y. Xiong and X. Lu, *Metallic Nanostructures*, Springer, Switzerland, 2015.

29 H. H. Kung, H. S. Jarrett, A. W. Sleight and A. Ferretti, *J. Appl. Phys.*, 1977, **48**, 2463.

30 S. H. Wemple, *Phys. Rev. B: Solid State*, 1970, **2**, 2679.

31 L. Hafid, *Solid State Commun.*, 1988, **66**, 841.

32 N. Szydlo and R. Poirier, *J. Appl. Phys.*, 1980, **51**, 3310.

33 J. Tang, M. White, G. D. Stucky and E. W. McFarland, *Electrochem. Commun.*, 2003, **5**, 497.

34 B. Enright and D. Fitzmaurice, *J. Phys. Chem.*, 1996, **100**, 1027.

35 P. Erhart and K. Albe, *J. Appl. Phys.*, 2007, **102**, 1.

36 T. Sekiya, K. Ichimura, M. Igarashi and S. Kurita, *J. Phys. Chem. Solids*, 2000, **61**, 1237.

37 H. Tang, F. Lévy, H. Berger and P. E. Schmid, *Phys. Rev. B: Condens. Matter Mater. Phys.*, 1995, **52**, 7771.

38 D. Bäuerle, W. Braun, V. Saile, G. Sprüssel and E. E. Koch, *Z. Phys. B: Condens. Matter Quanta*, 1978, **29**, 179.

39 M. R. Morris, S. R. Pendlebury, J. Hong, S. Dunn and J. R. Durrant, *Adv. Mater.*, 2016, **28**, 7123.

40 Y. Sun and R. J. Nemanich, *J. Appl. Phys.*, 2011, **109**, 104302.

41 J. N. Hanson, B. J. Rodriguez, R. J. Nemanich and A. Gruverman, *Nanotechnology*, 2006, **17**, 4946.